PHOTOCATALYTIC DEGRADATION OF TETRACYCLINE IN AQUEOUS SOLUTION BY ZnO QUANTUM DOTS/TiO_2 SUPPORTED CATALYSTS

USMAN SAIDU

UNIVERSITI SAINS MALAYSIA

2021

PHOTOCATALYTIC DEGRADATION OF TETRACYCLINE IN AQUEOUS SOLUTION BY ZnO QUANTUM DOTS/TiO_2 SUPPORTED CATALYSTS

by

USMAN SAIDU

Thesis submitted in fulfilment of the requirements
for the degree of
Doctor of Philosophy

March 2021

ACKNOWLEDGEMENT

I would like to extend my heartfelt gratitude to my supervisor, Dr. Mohammad Anwar Mohamed Iqbal, for his supervision, advice, guidance, and insightful comments throughout all stages of this research. I would also like to sincerely thank my co-supervisors, Prof. Dr. Farook Adam and Prof. Dr. Srimala Sreekantan for their important guidance and suggestions.

I also extend my sincere thanks to all the staff of School of Chemical Sciences, School of Physics, Science & Engineering Research Center (SERC), and Centre for Global Archeological Research, Universiti Sains Malaysia, for their supports especially for material characterizations. My appreciation to Dr. Noorfatimah of Advanced Medical and Dental Institute (AMDI), Universiti Sains Malaysia, for her guidance during LC-MS analysis. I would also like to thank my lab-fellows such as Tan Kok, Fateemah, Ruzaina, Hanisah, Norma and Mohamed for their togetherness.

I must express my gratitude to my parent, brothers and sisters for their constant encouragement and prayers. I do not have the words to express my feeling for my wife, Rukayya Zubair Abubakar and my children, who had to put up with my frequent absence in the course of this work. They were indeed understanding, and I acknowledge their patience, prayers, and other supports. May Allah reward everyone's effort. Ameen.

I would also like to thank Ministry of Education (MOE) for funding this project through Fundamental Research Grant Scheme (FRGS/1/2019/STG01/USM/02/7) and Transdisciplinary Research Grant Scheme (TRGS/1/2016/USM/01/4/1).

Finally, I also gratefully thank Sule Lamido University, Kafin Hausa for giving me the opportunity to travel all the way to Malaysia for my PhD study. I also thank the Tertiary Education Trust Fund (TETFund), Nigeria, for my scholarship.

TABLE OF CONTENTS

APPENDICES

LIST OF TABLES

LIST OF FIGURES

LIST OF SCHEMES

Page

LIST OF SYMBOLS

eV	Electron volt
g	Gram
µg	microgram(s)
h^+	Photogenerated hole
hν	Photonic energy
$O_2^{\bullet\,-}$	Superoxide radical
OH^-	Hydroxide ion
$OH^\bullet$	Hydroxyl radical

LIST OF ABBREVIATIONS

AA	Ascorbic acid
AFM	Atomic Force Microscopy
AOP	Advanced oxidation process
BET	Brunauer-Emmett-Teller
BJH	Barret-Joyner-Halenda
CB	Conduction band
DI	Deionized
DSC	Differential scanning calorimetric
e^-	Negatively charged electron
Eg	Bandgap
FESEM	Field emission scanning electron microscopy
FT-IR	Fourier transform infrared
h	Hour
HA	Humic acid
HRTEM	High resolution transmission electron microscopy
ICP-OES	Inductively coupled plasma optical emission spectrometry
IPA	Isopropanol
L	Liter(s)
LC/TOF/MS	Liquid chromatography/time-of-flight/mass spectrometry
LLDPE	Linear low-density polyethylene
M	Molar(s)
Max	Maximum
mg	Milligram(s)
Min	Minimum
min	Minute(s)

mM	Millimolar
mmole	Millimole(s)
NAD	Nitrogen adsorption-desorption analysis
ng	Nanogram(s)
nm	Nanometer(s)
NOM	Natural organic matter
NPs	Nanoparticles
PL	Photoluminescence
PZC	Point of zero charge
QCE	Quantum confinement effect
QDs	Quantum dots
RPM	Round per minute
TC	Tetracycline
TEA	Triethanolamine
TEM	Transmission electron microscopy
TEOS	Tetraethylorthosilicate
TGA	Thermogravimetric analysis
TOC	Total organic carbon
UV-Vis DRS	UV-Visible diffuse reflectance spectroscopy
UV-vis	Ultraviolet-visible
VB	Valence band
WWTP	Wastewater treatment plant
XPS	X-ray photoelectron spectroscopy
XRD	X-ray diffraction

LIST OF APPENDICES

DEGRADASI FOTOPEMANGKINAN TETRASIKLIN DALAM LARUTAN AKUEUS OLEH MANGKIN TERSOKONG TITIK KUANTUM ZnO/TiO_2

ABSTRAK

Dalam penyelidikan ini, nanopartikel TiO_2 (TiO_2 NPs) digabungkan dengan 3%, 5%, 8%, dan 10% ZnO QD melalui kaedah sol-gel. Fotopemangkin (xZnO QDs/TiO_2; x = 3%, 5%, 8% dan 10%) dicirikan menggunakan analisis pembelauan sinar-X (XRD), spektroskopi inframerah transformasi Fourier (FTIR), mikroskopi daya atom (AFM), mikroskopi penghantaran elektron beresolusi tinggi (HRTEM), mikroskopi pengimbasan medan pelepasan elektron (FESEM), spektroskopi pantulan difus ultra lembayung-nampak (UV-Vis DRS), Brunauer-Emmett-Teller (BET), spektroskopi fotoelektron sinar-X (XPS), dan fotolumisen (PL). Kecekapan fotopemangkin tersebut diuji dalam penguraian tetrasiklin (TC) di bawah sinaran cahaya nampak secara terampai. Kira-kira 95% penguraian TC dicapai dalam masa 90 minit di bawah sinaran cahaya nampak menggunakan 8%-ZnO QDs/TiO_2, di bawah keadaan optimum: kepekatan TC = 40 mg/L, pH = 9, dos pemangkin = 250 mg /L. Fotopemangkin nanokomposit 8%-ZnO QDs/TiO_2 seterusnya dipegunkan pada polimer polietilena linear berketumpatan rendah (LLDPE) menggunakan kaedah tuangan pelarut. Filem komposit dipegunkan dengan LLDPE (8%-ZnO QDs/TiO_2@LLDPE), yang mengandungi jumlah nanokomposit ZnO QDs/TiO_2 yang berbeza (2, 5, 8, dan 10 wt.%) dicirikan dengan FTIR, XRD, FESEM, AFM , DSC, TGA, sudut sentuhan air, dan analisis UV-vis-DRS. Kajian struktur dan morfologi menunjukkan bahawa nanokomposit tersebar secara homogen dan melekat pada matriks LLDPE. Filem tersebut menunjukkan kekasaran permukaan yang lebih tinggi dan lebih hidrofilik berbanding dengan filem LLDPE yang tulen. Aktiviti fotopemangkinan filem tersebut dinilai dalam penguraian TC di bawah sinaran cahaya nampak. Penekanan diberikan pada pengaruh muatan pemangkin, pH larutan, saiz filem, sumber cahaya, kajian kebolehgunaan semula mangkin, serta pengaruh ion takorganik dan bahan organik semula jadi (NOM) terhadap degradasi TC. Kesemua fotopemangkin yang disintesis mempamerkan kinetik tertib pseudo-pertama dengan filem fotopemankin terbaik mempunyai kecekapan 89.45% dibawah sinaran cahaya nampak selama 180 minit. Selain itu, filem fotopemangkin dapat dipisahkan dan digunakan kembali dengan mudah beberapa kali, menunjukkan potensi yang besar untuk aplikasi praktikal dalam rawatan air sisa. Akhirnya, produk degradasi TC dikaji dengan analisis kromatografi cecair spektrometri jisim masa terbang (LC/TOF/MS). Berdasarkan perantaran yang telah dikenal pasti, laluan penguraian fotopemangkinan TC dicadangkan.

PHOTOCATALYTIC DEGRADATION OF TETRACYCLINE IN AQUEOUS SOLUTION BY ZnO QUANTUM DOTS/TiO_2 SUPPORTED CATALYSTS

ABSTRACT

In this research, TiO_2 nanoparticles (TiO_2 NPs) were incorporated with 3%, 5%, 8%, and 10% ZnO quantum dots (ZnO QDs) *via* sol-gel method. The photocatalyts (xZnO QDs/TiO_2; x= 3%, 5% 8% and 10%) were characterized using X-ray diffraction (XRD), Fourier transform infrared spectroscopy (FTIR), atomic force microscopy (AFM), high resolution transmission electron microscopy (HRTEM), field emission scanning electron microscopy (FESEM), ultraviolet-visible diffuse reflectance spectroscopy (UV-vis DRS) Brunauer-Emmett-Teller (BET), X-ray photoelectron spectroscopy (XPS), and photoluminescence (PL) analyses. The synthesized photocatalysts' efficiency in suspended form was tested in the photodegradation of tetracycline (TC) under visible light irradiation. About 95% degradation of TC was achieved within 90 min of visible light illumination using 8%-ZnO QDs/TiO_2, under the optimized conditions: TC concentration = 40 mg/L, pH = 9, catalyst dosage = 250 mg/L. The 8%-ZnO QDs/TiO_2 nanocomposite photocatalyst was immobilized on linear low-density polyethylene (LLDPE) polymer using the solution casting method. The LLDPE supported composite films (ZnO QDs/TiO_2@LLDPE), each with a different amount of 8%-ZnO QDs/TiO_2 nanocomposite (2, 5, 8, and 10 wt.%) were characterized by FTIR, XRD, FESEM, UV-vis-DRS, AFM, water contact angle, differential scanning calorimetry (DSC), and thermogravimetric (TGA) analyses. Structural and morphological studies revealed that the nanocomposites were homogenously dispersed and embedded onto the LLDPE matrix. Moreover, the film photocatalysts exhibited higher surface roughness and enhanced hydrophilicity compared to bare LLDPE film. The photocatalytic activity of the film photocatalysts was evaluated on the degradation of TC under visible light irradiation. Emphasis was placed on the effect of catalyst loading, solution pH, film size, light sources, catalyst reusability, as well as the effects of inorganic ions and natural organic matter (NOM) on the degradation of TC. All the synthesized photocatalysts exhibited pseudo-first-order kinetics with the best film photocatalyst had 89.45% efficiency after 180 min of visible light irradiation. Moreover, the as-synthesized film photocatalysts could be easily separated and reused for eight times, showing great potential for practical applications in environmental wastewater treatment. Finally, TC degradation products were studied by liquid chromatography/time of flight/mass spectrometry (LC/TOF/MS) analysis. Based on the identified intermediates, the photocatalytic degradation pathways of TC were proposed.

CHAPTER 1

INTRODUCTION

1.1 Occurrence of pharmaceuticals in the aquatic environment

Over the last few decades, the demand for pharmaceutical products, such as analgesics, antibiotics, anti-inflammatory, lipid regulators, beta-blockers, and tranquillizers have been increasing rapidly in developing countries (Couto *et al.*, 2019). These pharmaceutical products are essential to improve life quality and lifespan of human beings and animals (Li and Shi, 2016). Large portions of these pharmaceuticals are stable and difficult to be destroyed by traditional wastewater treatment techniques such as chlorination adsorption, ozonation and membrane processes (Lee *et al.*, 2019). As a result, many of these pharmaceuticals have continuously been encountered in various kinds of waters such as wastewater, surface water, drinking water, groundwater and in the soil, sediments and sludge (Xu *et al.,* 2020). The long-term and the low-dose exposures to pharmaceutical compounds in the environment lead to adverse effects on the terrestrial and aquatic organisms including chronic toxicity, endocrine disruption and the occurrence of antibiotic resistance bacteria (Wang *et al.*, 2019b, Xu *et al.*, 2020).

Among the pharmaceutical compounds present in the environment, special attention has been given to antibiotics. Antibiotics belong to a class of pharmaceuticals applied in the medication of infections in humans beings and other animals and to increase feed efficiency and improve the growth rate in livestock (Daghrir and Drogui, 2013). Annual consumption of antibiotics in the world was estimated in 2010 to be above 63,151 tons and project to rise by 67% by the year 2030 (Van Boeckel *et al.*, 2015). About 30% to 90% of the consumed antibiotics enter the ecosystem as a parent compound or metabolites since they are rarely metabolized entirely in the body (Wang *et al.*, 2017a). Like any other pharmaceuticals, the occurrence of antibiotics in the aquatic environment has been associated with many negative consequences such as short-term and long-term toxicities, endocrine-disrupting effects, and the emergence of antibiotic resistance bacteria (Almasi *et al.*, 2016).

The antibiotics enter the ecosystem through urine and faeces of animals and humans, inappropriate disposal of the drugs, pharmaceutical production plants, wastewater and aquaculture (Felis *et al.*, 2020). Conventional wastewater treatment plants (WWTPs) are not constructed for the removal of antibiotics (Hu *et al.*, 2018). Subsequently, a variety of antibiotics are released repeatedly into the aquatic environment (Praveena *et al.*, 2018, Ngigi *et al.,* 2020). For instance, Hou *et al.,* reported about 2.6 – 32.0 mg/L of tetracycline (TC) residues in the final effluent from WWTPs (Hou *et al.,* 2016). Another study conducted in Putrajaya, Malaysia showed that several therapeutic classes of pharmaceuticals and personal care products were detected in tap water, in the range of 0.03 – 21.39 ng/L, with diclofenac having the highest concentration (21.39 ng/L), followed by triclosan (9.74 ng/L) and ciprofloxacin (8.69 ng/L) (Wee *et al.,* 2020). Furthermore, Mahmood et al. (2019) analyzed the presence of three different antibiotics (amoxicillin, levofloxacin and ciprofloxacin) in potable water from two water treatment plants in Baghdad city. Their results confirmed the presence of all the target antibiotics in both raw and finished water samples of the treatment plants. Ciprofloxacin was detected in 11 out of 36 water samples, with the maximum concentration of 1.312 µg/L in the finished water. Levofloxacin was detected in 9 water samples, with the maximum concentration of 0.177 µg/L. While amoxicillin was found in 1 sample at a concentration of 1.50 µg/L (Mahmood *et al.,* 2019). Some of the most commonly detected antibiotics and other prescription drugs in surface water around the world were compiled by Quesada *et al.* (2019) as presented in Table 1.1.

Table 1.1 Occurrence and concentrations of some pharmaceuticals in surface water around the world published in the literature (Quesada *et.al.,* 2019).

Class of pharmaceuticals	**Pharmaceuticals**	**Min (ng/L)**	**Max (ng/L)**	**Mean (ng/L)**	**Country**
Analgesic and Anti-inflammatories	Acetaminophen	0	1561.00	445.00	India
		354.00	508.00	430.00	Mexico
		0	9822.00	209.00	UK
	Diclofenac	0	15.49	3.95	Malaysia
		258.00	352.00	313.00	Mexico
		25.13	51.24	33.56	Portugal
	Ibuprofen	184.00	284.00	231.00	Mexico
		0	2302.00	662.17	India
		-	6593.00	830.00	Spain
Antibiotics	Erythromycin	0	6.49	1.31	Bangladesh
		10.20	183.00	55.02	China
		0	263.00	-	UK
	Metronidazole	0.05	13.51	2.74	Bangladesh
		19.26	114.24	56.19	Malaysia
		108.00	502.00	299.00	Mexico
	Trimethoprim	0.40	52.10	12.35	China
		0.02	0.33	0.10	Sweden
Antidepressants	Diazepam	-	-	24.30	China
		0	305.00	55.50	India
		-	12.00	3.00	Spain
Antiepileptic	Carbamazepine	0	5.80	3.30	France
		0	1346.00	412.50	India
		0.9	9.39	-	USA

Table 1.1 (Continued)

Beta-blockers	Atenolol	-	900.00	470.00	Spain
		4.00	10.00	7.00	Mexico
	Propranolol	0.18	8.47	-	Sweden
		0	64.90	11.66	UK
Anti-hyperglycemic	Metformin	0.20	121.40	34.73	China
		0.44	8.40	2.60	Sweden
		45.20	2595.00	677.00	UK
Stimulant	Caffeine	0	81.00	41.30	France
		0	2640.00	977.00	India
		16.27	36.00	30.83	Malaysia
		8.05	26.92	-	USA
Lipid regulators	Gemfibrozil	14.00	24.00	20.00	Mexico
		-	3735.00	77.00	Spain
		-	-	95.00	USA

1.2 Problems statement

Modification of TiO_2 via coupling with semiconductor quantum dots (QDs) possesses its unique advantages, considering its efficiency in suppressing electron-hole recombination and also increase the surface area of TiO_2, which enhances the efficiency of the photocatalytic process. As a common type of QDs, chalcogenide compound QDs, such as CdS QDs (Xu *et al.,* 2018), CdSe QDs (Chen et al., 2018b), and PbS QDs (Ikram *et al.*, 2016, Pathak *et al.,* 2018), have been employed as coupled semiconductors due to their ability to act as sensitizers or separation centres. However, the usage of heavy metal elements is a potential risk to water quality, because of the easy release of heavy metal ions from chalcogenide compounds during the undesired photocorrosion (Li *et al.,* 2019a, Aziz et al., 2019, Chen et al., 2020). Hence, it is imperative to develop a new catalyst devoid of the aforementioned hazardous properties. ZnO QDs exhibits potential for use as coupled semiconductors due to its non-toxicity, stability, low cost, easy acquisition and can increase the surface area of TiO_2, which enhances the efficiency of the photocatalytic process.

Many disadvantages of the use of photocatalyst in powder form have been noted. Such disadvantages include i) low light utilization efficiency of suspended photocatalyst, ii) difficulty and high cost in the separation and recovery of the catalyst from suspension, iii) aggregation of catalytic particles, especially at higher concentrations, and iv) possibility to cause adverse human health problems by the loose powder (Luo *et al.,* 2015, Teixeira *et al.*, 2016, Goutham *et al.,* 2019). To avoid the use of photocatalyst in powder form, several efforts have been made to immobilize photocatalyst on various substrates such as clay and ceramic (Kaur *et al.,* 2018, Yadav *et al.,* 2019), silica (Blanchard *et al.*, 2020), glass spheres (Cunha *et al.,* 2018), zeolite (Rangkooy *et al.,* 2019) and polymer (Reddy *et al.*, 2019). However, in most cases, the photocatalyst degrades the organic pollutants and the support material in which the photocatalyst are embedded. Hence, the choice of reliable support and its inertness is always of paramount importance.

The degradation and subsequent mineralization of antibiotics would produce carbon dioxide, water, and other nontoxic compounds as the final products. During the degradation process, antibiotics pollutant is attacked by the active species generated by the photocatalyst and oxidized into intermediates which could be more toxic than the final products. Therefore, it is necessary to know the intermediates formed during the photocatalytic degradation of antibiotics to ensure full conversion into harmless compounds.

1.3 Research objectives

Based on the aforementioned issues, the objectives of this research are:

1. To synthesize and characterize ZnO QDs, TiO_2 NPs and ZnO QDs/TiO_2 nanocomposites photocatalysts.
2. To prepare and characterize linear low density polyethylene (LLDPE) supported ZnO QDs/TiO_2 nanocomposites photocatalysts.
3. To investigate the potential of the synthesized materials for the degradation of TC under visible light irradiation.
4. To identify the degradation products using liquid chromatography/time-of -flight/mass spectrometry (LC/TOF/MS) analysis.
5. To establish plausible TC degradation pathways.

1.4 Thesis outline

The entire thesis is divided into seven chapters and organized as follows:

Chapter 1 provides a brief overview of the background information issues related to the presence and impact of pharmaceuticals in the environment, outlying the importance of removing these compounds from water. It emphasized on the problem statement, research objectives and the outline of this thesis.

Chapter 2 presents a comprehensive literature review concerning the advanced treatment technologies for the removal of pharmaceuticals with special emphases on heterogeneous photocatalysis. The chapter also discussed the mechanism of TiO_2 photocatalysis, as well as various approaches for the modification of TiO_2. . Furthermore, in this chapter, the advantages and limitations of catalyst immobilization techniques were discussed. Finally, the potential applications of these photocatalytic materials were explained.

Chapter 3 outlines the details about the materials and methods employed in this study. The principles of instrumental characterization methods were also discussed. Moreover, the methodology used to assess the photocatalytic degradation process was described.

Chapter 4 discussed the detailed characterizations of the as-synthesized nanocomposite photocatalysts through XRD, FTIR, AFM, SEM, TEM, HR-TEM, N_2-sorption analysis, ICP-OES, PL and XPS analyses.

Chapter 5 evaluated the photocatalytic activity of the as-prepared ZnO QDsTiO_2 nanocomposite photocatalysts on the degradation of TC. The different factors affecting TC degradation were assessed to determine the optimum conditions for the complete degradation of TC. Furthermore, the scavenging experiments and the main mechanism involved in the degradation of TC were discussed. Moreover, the reusability and the degree of mineralization of the as-synthesized ZnO QDs/TiO_2 nanocomposite photocatalyst on TC's degradation was evaluated. Finally, TC degradation intermediates were detected by LC/TOF/MS analysis, and plausible TC degradation pathways were proposed.

Chapter 6 discussed the detailed characterizations of the LLDPE supported ZnO QDs/TiO_2 composite films. The performance of the as-prepared LLDPE composite films on the degradation of TC was evaluated. Effects of some operational parameters such as initial pH, film size, light sources, inorganic ions, and natural organic matter (NOM) on the TC degradation by the LLDPE composite films were evaluated. Furthermore, the reusability and the TC degree of mineralization by the LLDPE composite films were evaluated and discussed. Finally, TC degradation intermediates were detected by LC/TOF/MS analysis, and plausible TC degradation pathways were proposed.

Chapter 7 concludes the overall research findings and makes some recommendations for future studies.

CHAPTER 2

LITERATURE REVIEW

2.1 Advanced treatment technologies for pharmaceuticals removal

During the past decade, various approaches such as ion exchange, adsorption, nanofiltration, reverse osmosis, ultrafiltration, ozonation, aerobic treatment, photo-Fenton, electrochemical oxidation, and photocatalysis have been employed to remove pharmaceuticals from aqueous media (Moreira *et al.,* 2018, Lan *et al.*, 2019, Mora-Gomez *et al.*, 2019, Mahmoud *et al.*, 2020, Zhou *et al.*, 2020). Despite that these methods have shown some efficiency on the removal of antibiotics in aqueous solution, most of them have some limitations. Anaerobic biological treatment could not effectively remove antibiotics residue in wastewater due to its bacterial resistance. As a result, it leads to incomplete degradation of the antibiotics or its adsorption to sludge (Wu *et al.*, 2020). Membrane processes like nanofiltration (NF) and reverse osmosis (RO) also have some limitations, such as membrane fouling and high energy consumption. Other problems of membrane processes include non-applicability in treating large volumes of pollutant and difficulty in safe disposable of the concentrated stream (de Andrade *et al.,* 2018). Activated carbon adsorption using powdered activated carbon (PAC) and granular activated carbon (GAC) has been reported to be active in removing pharmaceuticals. However, these methods do not destroy pollutants but concentrating them and solely cause a phase transfer of contaminants, producing highly secondary waste pollutants which require further treatment (Cai *et al.*, 2020). Moreover, the presence of natural organic matter (NOM) significantly decreases the adsorption process's efficiency. The NOM could compete with target compounds for active binding sites, leading to pore blockage. The extensively used thermal regeneration of spent activated carbon is expensive and indirectly causes additional environmental pollution (Yao *et al.,* 2020).

Advanced Oxidation Processes (AOPs) are considered as the most effective technique for removing pharmaceuticals from wastewaters. AOPs degrade the pharmaceuticals into simpler or non-toxic compounds rather than concentrating or physically removing them as in adsorption and membrane processes. The AOPs are broadly defined as the techniques involving the generation of sufficient hydroxyl radicals ($^{\bullet}OH$) for water purification. AOPs do not generate wastes and can be applied as a pre-treatment process before the biological treatment, which can enhance the biodegradability of refractory compounds (Mirzaei *et al.*, 2017). Various types of water pollutants such as pesticides, pharmaceuticals and pathogens could be adequately treated by using AOPs. Prominent AOPs include Fenton, photo-Fenton, ozonation, sonolysis, UV and UV/H_2O_2 oxidation, electrochemical oxidation and photocatalysis. These can further be classified as homogeneous oxidation or heterogeneous oxidation processes.

The homogeneous oxidation process refers to the existence of both reactants and the photocatalysts in the same phase. The homogeneous oxidation generally refers to the reactants and the photocatalysts existing in the same phase. It can be classified into ozonation, Fenton and photo-Fenton reactions. In the ozonation process, strong oxidant ozone (O_3) is used, which decomposes in water, forming highly reactive $^{\bullet}OH$. Ozonation is preferred in alkaline condition due to the increase in the production of $^{\bullet}OH$ at this condition. Combination of O_3 and peroxide (O_3/H_2O_2) or UV (O_3/UV) as shown in equations 1.1 and 1.2 have been reported to improve the efficiency of the ozonation process (Fernandes *et al.*, 2019). However, the short lifetime of O_3 cause the ozonation process to be costly, and its high-energy intensity has also been identified as a drawback. Besides, the ozonation process is suspected to generate carcinogenic and unregulated by-products such as bromate (BrO^{3-}) (Reddy *et al.,* 2018).

$$H_2O_2 + 2O_3 \rightarrow 2OH^{\bullet} + 3O_2 \quad (2.1)$$

$$O_3 + hv + H_2O \rightarrow 2OH^{\bullet} + O_2 \quad (2.2)$$

Fenton reaction involves generating hydroxyl radicals through the decomposition of H_2O_2 by Fe^{2+} ions present in the aqueous phase, as shown in equation (1.3). The catalyst can be recovered, as shown in equation (1.4) or by the reaction of Fe^{3+} with other intermediates (Zhang *et al.*, 2019b). The oxidation rate in Fenton reaction is affected by many factors such as pH value, the ratio of Fe^{2+} to H_2O_2, and the amount of iron salt. Even though Fenton's reagents are simple and easy to apply without any energy input requirement, there are many problems associated with the process. Such problems include the risk of storage of H2O2, narrow working pH range, and iron sludge building, leading to secondary pollution (Jain *et al.*, 2018, Zhang *et al.*, 2019b).

$$Fe^{2+}_{(aq)} + H_2O_2 \rightarrow Fe^{3+}_{(aq)} + OH^- + HO^{\bullet} \quad (2.3)$$

$$Fe^{3+}_{(aq)} + H_2O_2 \rightarrow Fe^{2+}_{(aq)} + HO_2^{\bullet} + H^+ \quad (2.4)$$

Photo-Fenton reaction is the combination of Fenton's process with UV light. In photo-Fenton process, the rate of hydroxyl formation enhances compared to Fenton reaction. The essence of the photo-Fenton process is to regenerate Fe^{2+} from Fe^{3+} using light energy (Zhang *et al.,* 2019b). The effectiveness of the photo-Fenton process in the degradation of pharmaceuticals has been reported by several researchers (Serpone *et al.*, 2017, Serna-Galvis *et al.,* 2017). However, some disadvantages, such as low utilization rate of light energy and requiring an additional separation step to remove iron species after treatment, limits its applications.

Heterogeneous photocatalysis can be defined as a type of photoreaction in which the reactant and the photocatalyst exist in different phases, and where reactions occur on the surface of the photocatalyst. The heterogeneous photocatalytic process has received increased attention recently as a result of its effectiveness in rapidly degrading organic pollutants into less toxic compounds. This type of photocatalysis will be described in detail in the next section.

2.2 Heterogeneous photocatalysis

Heterogeneous photocatalysis employs inorganic semiconductors, such as ZnO, Bi_2O_3, SnO_2, ZrO_2, MoS_2, CdS, WO_3 and TiO_2, which upon irradiation with light (*hv*) of energy equal or greater than the bandgap energy of the semiconductor can create electron/hole pairs (e^-/h^+). Hence, the electrons are excited from the filled valence band (VB) to the empty conduction band (CB) of the semiconductor, leaving a positive hole in the valence band (Li and Shi, 2016). Some electrons and holes can migrate to the surface of the semiconductor without recombination and commence redox reactions with water and the oxygen adsorbed on the photocatalyst surface, resulting in the degradation and subsequent mineralization of pollutants, as schematically presented in Figure 2.1

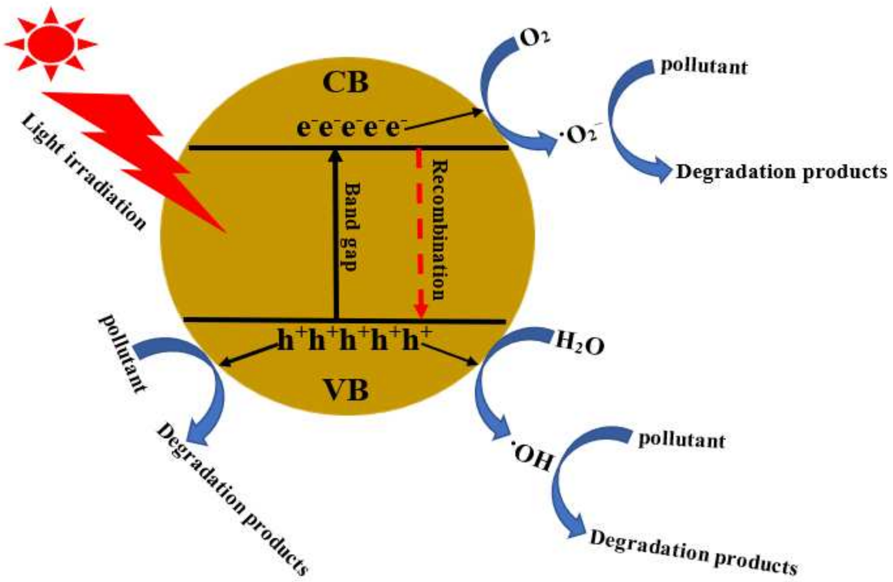

Figure 2.1 The schematic diagram of a semiconductor photocatalytic degradation (Li and Shi, 2016).

Generally, the heterogeneous photocatalytic process consists of four successive steps, namely, (i) light-harvesting, (ii) photogeneration of charges, (iii) charge transfer and recombination, and (iv) oxidation-reduction reactions. It is pertinent to know that a decrease in the fractional performance at any step might cause a reduction in the overall efficiency of the photocatalytic process. For instance, higher light reflection is expected if the surface of the photocatalyst is even and smooth, which is disadvantageous for light-harvesting and pollutant absorption. Highly uneven and porous photocatalysts allow the multiple reflections and scattering of light within the interiors of cavities and inside their pore channels, resulting in the enhancement of light utilization and generating more photoexcited e^{-}/h^{+} pairs to enhance the photocatalytic efficiency. Moreover, rapid recombination of photoexcited e^{-}/h^{+} pairs on the photocatalyst surface is another important aspect hindering photocatalytic process enhancement. The fast recombination of charge carriers is among the most critical and challenging aspect of heterogeneous photocatalysis. Lastly, significant agglomeration of nanostructured particles leads to a low specific surface area, which reduces the rate of reduction and oxidation processes. It further increases the diffusion boundaries of the reagents. All these are disadvantageous for the improvement of the photocatalytic process.

On the other hand, for the photodegradation of organic pollutants in aqueous solutions, the enhanced rate of adsorption and diffusion of reactants in a porous photocatalyst might still significantly enhance the efficiency of the photocatalyst due to the decrease in mass-transport boundaries and a higher rate of activation of the adsorbed species. All the factors as mentioned earlier in the heterogeneous photocatalytic process have been demonstrated to control the photocatalysts' general performance significantly. Regarding their usage practically, these factors must be handled skillfully to enhance the photocatalytic process's efficiency (Li *et al.,* 2016).

From a thermodynamic perspective, the photocatalytic redox reactions are driven by the photoinduced e^- and h^+, respectively, provided their reduction and oxidation potentials fall between the CB and the VB potentials. The energy of the conduction band edge (E_{CB}) corresponds to the potential of the photogenerated electrons, while the energy of the valence band (E_{VB}) corresponds to the potential of the holes. If E_{CB} is more negative than the potential of a species presents in solution, electrons reaching the surface of the semiconductor can reduce the oxidized form of the redox couple. On the other hand, if the valence band's potential is more positive than that of the redox couple, photogenerated holes can oxidize its reduced form. Thus, the knowledge of the relative edge positions of the bands and that of the energetic levels of the redox couples is essential to establish if thermodynamics allows the occurrence of the reactions with the photogenerated species on the catalyst surface, to generate reactive species which degrade the organic contaminants. The redox potentials of different species at pH = 7, are given in Figure 2.2. The potentials of the VB and theCB edges of a semiconductor can be calculated using Mulliken electronegativity theory as shown in equations 1.5 and 1.6 (Suyana *et al.*, 2017).

$$E_{VB} = X - E^e + 0.5Eg \tag{2.5}$$

$$E_{CB} = E_{VB} - Eg \tag{2.6}$$

Where, E_{VB} is the valence band edge potential, E_{CB} is the conduction band potential, Eg is the bandgap of the semiconductor, E^e is the energy of free electrons on the hydrogen scale (~4.5 eV) and X is the electronegativity of the semiconductor, obtained by summing the electronegativity of each atom in the semiconductor. Thus, the more negative CB positions of a photocatalyst are favourable for the reduction reactions, while the more positive VB positions of semiconductors are beneficial for oxidation reactions.

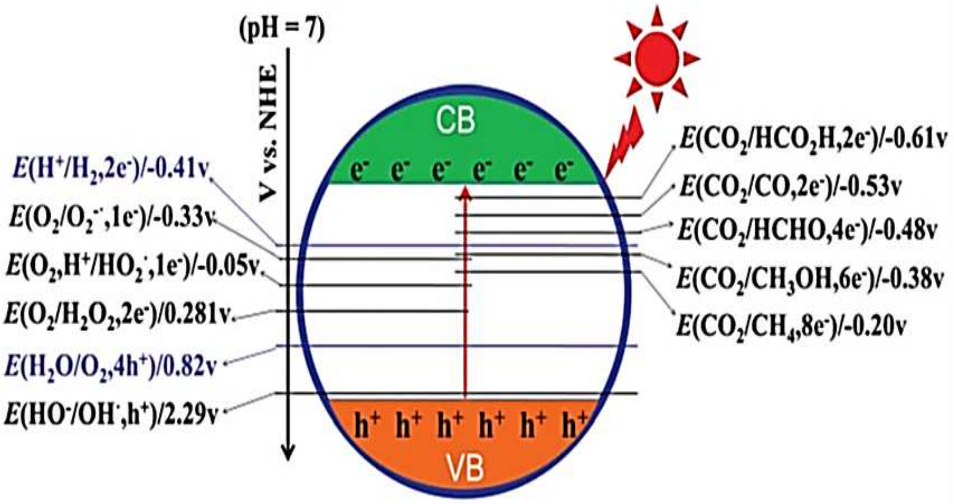

Figure 2.2 The redox potentials of different species in heterogeneous photocatalysis (Li *et al.*, 2016).

Numerous semiconductors such as PbS, CdS, ZnS, WO_3, SnO_2, and ZnO have been tested for heterogeneous photocatalysis, especially for environmental remediation. However, titanium dioxide (TiO_2) is the most widely used semiconductor due to its outstanding properties such as stability, non-toxicity, and inexpensive and inertness, and therefore, it is generally considered the best photocatalyst material.

2.2.1 Titanium dioxide (TiO_2) as photocatalyst

TiO_2 is a metal oxide with a molecular weight of 79.90 g mol^{-1} and classified as non-hazardous by the United Nation (UN) Globally Harmonized System (GHS) of Classification and Labelling of Chemicals (Abdullah and Kamarudin, 2015). Amongst all the available photocatalysts, TiO_2 has been investigated most extensively.

TiO_2 possess three crystalline polymorphs in nature, namely anatase, rutile and brookite (Figure 2.3) (Tran *et al.*, 2017); their structures are shown in Figure 1.3. All three polymorphs are composed of a titanium atom surrounded by six oxygen atoms in a more or less distorted octahedral configuration. The overall variation in the linking style of this TiO_6 is the fundamental difference between these three polymorphs. This connections pattern usually determines the crystal structure, surface structure, and electronic structure of TiO_2 photocatalyst materials. For instance, the differences in lattice structures of anatase and rutile TiO_2 cause different densities and electronic band structures, leading to different band gaps for bulk materials: anatase 3.20 eV and rutile 3.02 eV. Therefore, pure TiO_2 is primarily active under UV light. Amongst these three forms, rutile is the most stable phase of TiO_2, followed by anatase and brookite, which are metastable and can be transformed to rutile when heated at temperatures between 550 ºC and 1000 ºC (Reyes-Coronado *et al.*, 2008). Anatase can exhibit higher photocatalytic activity than rutile or brookite, due to its efficiency in light-harvesting and prolong the lifetimes of charge carriers, slightly higher Fermi level. Another reason is that anatase has a higher degree of hydroxylation (i.e., number of hydroxyl groups on the surface) (Ma *et al.*, 2016). On the other hand, the rutile phase suffers from weaker adsorption of organic pollutants and faster recombination of electron-hole pairs, while brookite is challenging to synthesize (Hezam *et al.,* 2019). In recent years, some studies revealed superior photocatalytic activity of mixed-phase TiO_2, such as anatase-rutile (Wang *et al.*, 2018d). The superior photocatalytic activity of this mixed-phase TiO_2 results from the effective transfer of photo-generated electrons from the CB of anatase to that of rutile, favoring electron-hole separation.

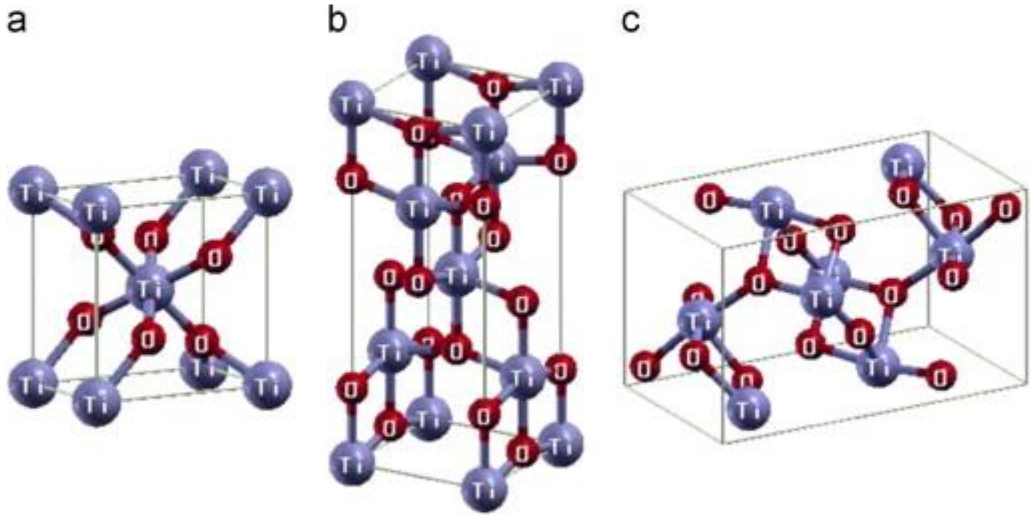

Figure 2.3 The crystal structures of (a) rutile (b) anatase and (c) brookite (Mohamad *et al.,* 2015).

2.2.2 Mechanism of TiO_2 photocatalysis

When the light of energy equal to or higher than the bandgap energy of TiO_2, the electron/hole pair is generated. The absorption of a photon excites an electron to the CB (e_{CB}^-) generating a positive hole in the VB (h_{VB}^+) (equation 2.7). As these photogenerated electrons and holes are unstable, most of them recombine and release energy as heat (equation 2.8), limiting the application of TiO_2 catalyst.

$$TiO_2 + hv \rightarrow TiO_2(h_{VB}^{+} + e_{CB}^{-}) \quad (2.7)$$

$$h_{VB}^{+} + e_{CB}^{-} \rightarrow heat \quad (2.8)$$

The photogenerated holes in the valence band can oxidize water adsorbed at the surface of the TiO_2 to produce hydroxyl radical ($^{\bullet}OH$) (equation 2.9), which are highly reactive towards organic molecules. The hydroxyl radicals can subsequently oxidize organic species with mineralization producing carbon dioxide and water (equation 2.10).

$$H_2O + h_{VB}^{+} \rightarrow OH^{\bullet} + H^{+} \quad (2.9)$$

$$OH^{\bullet} + pollutant \rightarrow H_2O + CO_2 \quad (2.10)$$

The photogenerated electrons in the conduction band can rapidly be trapped by molecular oxygen adsorbed on the titania particle, which is reduced to form superoxide radical anion ($O_2^{\bullet -}$) (equation 2.11). The superoxide radical anion formed may further react with H^+ to generate hydroperoxyl radical ($^{\bullet}OOH$) (equation 2.12), which also reduced to H_2O_2 (equation 2.13). Any of these reactive oxygen species may contribute to the oxidative pathways such as the degradation of organic pollutant (equations 2.14 and 2.15).

$$O_2 + e_{CB}^{-} \rightarrow O_2^{\bullet -} \quad (2.11)$$

$$O_2^{\bullet -} + H^{+} \rightarrow HOO^{\bullet} \quad (2.12)$$

$$HOO^{\bullet} + HOO^{\bullet} \rightarrow H_2O_2 + O_2 \quad (2.13)$$

$$O_2^{\bullet -} + pollutant \rightarrow H_2O + CO_2 \quad (2.14)$$

$$HOO^{\bullet} + pollutant \rightarrow H_2O + CO_2 \quad (2.15)$$

The appropriate energy band alignment of TiO_2 will insure the concurrent generation of reactive species such as $^{\bullet}OH$, $O_2^{\bullet-}$ h^+ and H_2O_2, which can degrade organic pollutants into various intermediates. These intermediates then go through a series of degradation processes and could result in complete mineralization forming carbon dioxide and water. The overall mechanism of TiO_2 photocatalysis can be described by equation 2.16.

$$Pollutant + TiO_2 + hv \rightarrow intermediates \rightarrow H_2O + CO_2 \tag{2.16}$$

The results of photocatalytic degradation reactions are mostly presented in terms of the decrease in the concentration of the pollutant as a function of time, in the presence of the photocatalyst under UV or visible light irradiation.

2.2.3 Kinetics of TiO_2 photocatalytic degradation

Previous studies have suggested that the pseudo-first-order kinetics model is best employed to describe the photocatalytic degradation of different organic compounds, especially antibiotics (Safari *et al.,* 2015). In general, the rate of heterogeneous catalytic reactions is explained under the conditions of the Langmuir-Hinshelwood (L-H) kinetic model (Eslami *et al.*, 2016) as follows:

$$r = -\frac{dc}{dt} = \frac{kKC}{(1 + KC)} \tag{2.17}$$

where,

r = initial rate of photooxidation

C = concentration of organic compound

T = irradiation time

k = rate constant

K = adsorption coefficient of the organic compound.

For solutions with a very low concentration (e.g., antibiotics in water) K<< 1, the L-H equation is simplified into pseudo-first-order kinetics as follows:

$$-\frac{dC}{dt} = \mathrm{k}C \qquad (2.18)$$

$$ln\left(\frac{C}{C_0}\right) = -\ \mathrm{kt} \qquad (2.19)$$

Where,

k = reaction rate (min^{-1})

t = irradiation time (min)

C_0 = initial concentration of the antibiotic (mg/L)

C = final concentrations of the antibiotic (mg/L).

A plot of ln C_0/C versus time will give a straight line with a slope of k.

2.3 Modification of TiO_2 photocatalyst

Recombination of photogenerated charge carriers and the inability to utilize visible light are the major limitations in TiO_2 photocatalysis as it reduces the overall quantum efficiency (Huang *et al.*, 2016). Various approaches have been suggested to enhance the electron-hole separation and migration to improve the efficiency of TiO_2 photocatalysis. The approaches can be categorized as either morphological modifications, such as reducing particles size to nanoscale and porosity or as chemical modifications, by incorporating additional components in the TiO_2 structure. Therefore, the bandgap of catalyst can decrease, or recombination of photogenerated electron/hole pairs can prevent effectively.

2.3.1 Doping of metals and non-metals

Doping refers to the introduction of impurities (dopants), which are usually ions or atoms, into the interior structures of TiO_2 photocatalyst. Depending on different dopants, doping can be classified as metal doping or non-metal doping. The dopant species are usually fused into the lattice structure of TiO_2 to decrease the bandgap value by either lowering the upper CB edge or raising the lower VB edge, which sensitizes the TiO_2 to visible light active.

Modifications of TiO_2 with metal dopants which may be anions, cations, or transition metals ions have stretched out the spectral response of TiO_2 into the visible region and also improving its photocatalytic efficiency (Basavarajappa *et al.*, 2020). For instance, For instance, when metal ions enter the TiO_2 lattice, impurity levels forms in the band gap of TiO_2, which will narrow the band gap of TiO_2 and enhance the light absorption range . Moreover, metal ion doping affects the photocatalytic activity of TiO_2 by acting as a sink for the photogenerated charge carriers, hence reducing the recombination rate (Li and Shi, 2016).

Doping of TiO_2 with non-metal elements with high electronegativities and high ionization energies like boron, carbon, nitrogen, sulfur, fluorine and chlorine is a practical approach to enhance the visible light photoactivity, due to the bandgap narrowing and the shift of absorption edge (Huang *et al.,* 2016). The basic idea is that the non-metal dopants influence the VB through interaction with the O $2p$ electrons. The localized states or p states of non-metal dopants generally form the impurity levels above VB, which extends the optical absorption edge of TiO_2. Non-metal ions are less likely to form recombination centres when compared with metal ions. Therefore, non-metal dopants will not consume the photogenerated charges and are thus, more effective for improving photocatalytic activity (Li and Shi, 2016). For instance, the occurrence of surplus of either electrons or holes is likely to reduce the amount of photogenerated charges carriers; hence, decrease the efficiency of the photocatalyst, which is one of the major disadvantages of metal doping (Li and Shi, 2016). Other drawbacks associated with metal doping is that transition metals may lead to partial blockage of TiO_2 pores or causes particles growth, which would decrease the specific surface area of TiO_2 and, finally, the photocatalytic degradation performance (Shayegan *et al.*, 2018). The high cost of noble metal is another disadvantage of metal loading. Moreover, it is inevitable for the metal ion dopants to dissolve in the solution, which may be more toxic than the pollutant substrates (Gong *et al.*, 2018). On the other hand, non-metal doping has some disadvantages. For instance, doping non-metal into the TiO_2 lattice causes oxygen vacancies, becoming a significant recombination centre for charge carriers. Additionally, the doping procedure of non-metal dopants requires high temperatures thermal treatment or a long preparation time requiring high energy (Shayegan *et al.*, 2018).

2.3.2 Semiconductor coupling

Compared to doping, the semiconductors heterojunction system has attracted great attention. The system is an effective strategy to separate e^-/h^+ into different semiconductors, thereby enhancing the photocatalytic performance (Li and Shi, 2016). Depending on the electronic affinity and relative band gaps, semiconductors heterojunction can be categorized into three groups presented as type I, type II, and type III heterojunctions, as shown in Figure 2.4.

In the case of type-I heterojunction, photogenerated charges in both semiconductors accumulate in the same semiconductor with a narrower bandgap. Hence, no enhancement in charge separation can be expected. For type-II heterojunction, the staggering energy band arrangement makes the flow of charge carriers possible at the two semiconductors' interface, thus facilitating electron/hole separation. While in type-III heterojunction, the more apparent difference in VB and CB positions requires an extensive amount of energy for photoinduced charge transfer. Hence, type-II heterojunction is believed to exhibit the most potential in attaining the best photocatalytic efficiency as the alignment can adequately inhibit the electrons and holes recombination.

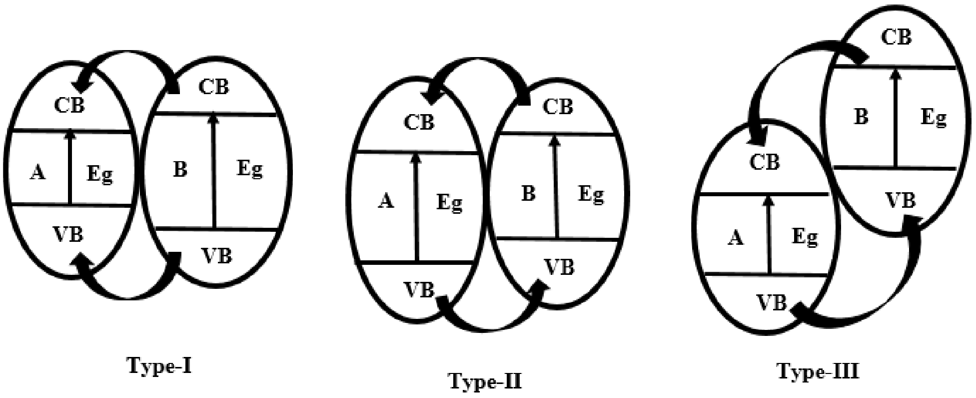

Figure 2.4 The schematic energy band diagram of three types of semiconductor heterojunctions (Humayun *et al.,* 2018).

Recently, numerous studies have directed on the development of type-II heterojunction photocatalyst (Humayun *et al.,* 2018). The following discussions will focus on the type-II heterojunctions unless otherwise stated. Depending on the movement of charge carriers as well as energy bands, type-II heterojunction comprises of three types of mechanisms, namely, conventional heterojunction, p-n heterojunction, and Z-scheme heterojunction.

2.3.2(a) Conventional heterojunction

In a conventional heterojunction, the photogenerated electrons transfer from semiconductor A to semiconductor B, due to the more negative CB position of semiconductor A. Concurrently, due to the more positive VB position of semiconductor B, photogenerated holes can transfer from semiconductor B to semiconductor A, resulting in efficient charge separation. Two possible cases could occur when coupled semiconductors are irradiated with light. In the first case, both semiconductors A and B responds to light irradiation, generating electrons and holes. A vectorial migration of electrons and holes from one semiconductor to the other occurs. In the second case, only semiconductor (B) is activated while semiconductor (A) is non-activated. Semiconductor A not activated because the light irradiated is insufficient to activate it. The photogenerated e^-/h^+ pairs are only generated in the semiconductor (B), the electron is migrated to the CB of semiconductor A, while the photogenerated h^+ remains in the VB of semiconductor (B), as shown in Figure 2.5 (a-c). However, in both cases, electrons and holes will be effectively separated in different semiconductors, leading to better photocatalytic performance. Van *et al.,* synthesized SnO_2/TiO_2 heterojunction photocatalyst system via the one-step hydrothermal method, and the photoactivity of the catalysts was tasted towards the degradation of methylene blue (MB) under simulated sunlight illumination. The SnO_2/TiO_2 heterojunction photocatalysts displayed significantly improved photocatalytic performance when compared with pure SnO_2 and TiO_2. The successful formation of heterojunction did not only enhance the separation of the photogenerated charge, but also a two-fold increase in the specific surface area of SnO_2/TiO_2 compared with pristine TiO_2 was obtained, resulting in efficient degradation of MB (Van Viet *et al.*, 2018).

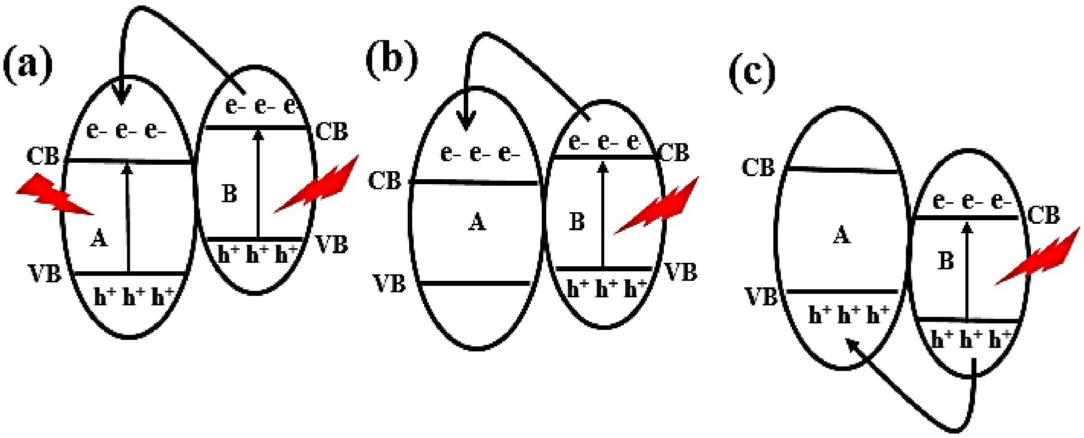

Figure 2.5 The transfer of photogenerated carriers in conventional heterojunction when both semiconductors are excited (a), only one semiconductor is excited (b) and (c).

2.3.2(b) p-n Heterojunction

Despite that the conventional heterojunctions can spatially separate the photogenerated e^-/h^+ pairs, the attained improvement in the e^-/h^+ pair separation is not enough to overcome the very fast e^-/h^+ pair recombination in the semiconductor. Hence, a p–n heterojunction photocatalyst system was introduced, which can accelerate the e^-/h^+ pair transfer across the heterojunction by providing an additional electric field (Zhang *et al.*, 2017). The p-n heterojunction system is usually formed between two types of semiconductors, p-type and n-type. Generally, prior to light irradiation, the electrons on the n-type semiconductor near the p–n interface tend to diffuse into the p-type semiconductor, leaving a positively charged species. Meanwhile, the p-type semiconductor holes near the p–n interface tend to diffuse into the n-type semiconductor, leaving a negatively charged species. The electron-hole diffusion will continue until the Fermi level equilibrium is achieved. As a result, the region close to the p–n interface is charged, generating an internal electric field as